Appl Phys B (2011) 102: 689–694
DOI 10.1007/s00340-010-4355-5

Applied Physics B
Lasers and Optics

Effects of a rectangular aperture on the vectorial structure of a Gaussian beam in the far-field regime

J.W. Tang · S.X. Li · T.F. Wang · K.C. Zhu

Received: 28 April 2010 / Revised version: 16 August 2010 / Published online: 12 January 2011

Abstract With the help of the angular spectrum representation and the Gaussian function expansions of the hard-edge aperture function, the vectorial structure of a linearly polarized Gaussian beam (GB) diffracted by a rectangular aperture is analyzed in detail. It is found that the sizes of the energy flux density spots and the energy fluxes of the TE and TM terms depend on the aperture configuration and the polarization direction of the incident GB. The far fields may have smaller spots and larger energy fluxes for a GB diffracted by a rectangular aperture compared to that by a square aperture with the same beam intensity. And another potential application in information encoding and transmission for free-space communications is also proposed in addition to re-focusing to enhance the optical storage density. This encoding scheme has the benefit of easy implementation without modulating any properties of the light source.

1 Introduction

The Gaussian beam (GB) is often encountered in laser optics and its propagation has been studied extensively within the framework of the paraxial approximation [1]. In practical optical systems, apertures are the most fundamental optical elements and commonly applied; therefore, the aperture effects on the beam propagation have received a large amount of attention and have been studied using a great number of different methods [2–8]. Within the non-paraxial framework, the far-field properties of an apertured GB have been analyzed using the scalar angular spectrum method [9, 10]. Since Lax et al. [11] pointed out the incompatibility of the paraxial solution with the exact Maxwell equations, a variety of non-paraxial approaches have been developed to describe the beam propagation beyond the paraxial approximation [12–16]. Based on the vectorial Rayleigh diffraction integral, the approximate analytical expression for the propagation equation of an apertured vector GB has been derived [17, 18]. Recently, by means of the vectorial angular spectrum method, vectorial structures of a few propagation beams have been revealed in the far field [19–31]. For example, the effect of a circular aperture on the vectorial structure of a GB was analyzed in detail [31]. Moreover, the equivalence between the vectorial angular spectrum representation and Rayleigh–Sommerfeld diffraction formulae was demonstrated [32].

In this paper, by expanding the aperture function as a sum of finite-term complex Gaussian functions [33] and with the help of the vectorial angular spectrum representation, the vectorial structure of a GB diffracted by a rectangular aperture is represented as an integral form. By means of the method of stationary phase, the analytical expressions of the TE and TM terms are obtained in the far field. The influence of the rectangular aperture and a linearly polarized angle on the vectorial structure of an apertured GB is investigated in the far field. In Sect. 2, analytical expressions of a linearly polarized GB diffracted at a rectangular aperture are derived. Numerical results of the energy flux densities of TE and TM terms and the whole field are presented in Sect. 3 to illus-

J.W. Tang · T.F. Wang
School of Physics, Hunan University of Science and Technology, Xiangtan 411201, Hunan, PR China

S.X. Li
Physical Staff Room, Guangdong Medical College, Dongguan 523808, Guangdong, PR China

K.C. Zhu (✉)
School of Physical Science and Technology, Central South University, Changsha 410083, Hunan, PR China
e-mail: kczhu058@mail.csu.edu.cn

trate how the rectangular aperture configuration and the polarization direction of an incident GB affect the propagation properties of diffracted fields. In Sect. 4, the energy fluxes of TE and TM terms are calculated and a comparison between them for a rectangular aperture and for a square aperture is performed. And, an encoding scheme is proposed to implement information transmission and communication in free space. Finally, a brief summary of the main results concludes this paper.

2 Analytical expression for GBs diffracted by a rectangular aperture

In the Cartesian coordinate system, assuming that a rectangular aperture is placed at the plane $z = 0$ and an incident plane wave is linearly polarized, the field of such an incident beam just behind the aperture reads

$$\begin{pmatrix} E_x(x, y, 0) \\ E_y(x, y, 0) \end{pmatrix} = \begin{pmatrix} \cos\alpha \\ \sin\alpha \end{pmatrix} \exp\left(-\frac{x^2 + y^2}{w_0^2}\right) \Pi(x, y), \tag{1}$$

where the window function of the rectangular aperture $\Pi(x, y)$ is expressed as

$$\Pi(x, y) = \begin{cases} 1 & |x| \le a,\ |y| \le b, \\ 0 & \text{otherwise.} \end{cases} \tag{2}$$

Here w_0 is the beam width, a and b are respectively the width and height of the rectangular aperture, the Jones vector $\binom{\cos\alpha}{\sin\alpha}$ describes the linearly polarized state of the incident plane wave, α is the linearly polarized angle with the x-axis and $k = 2\pi/\lambda$, with λ representing the wavelength of the incident plane wave. Here the time-dependent factor $\exp(-\mathrm{i}\omega t)$ (ω being the circular frequency) and the constant amplitude factor are suppressed in (1).

In order to arrive at the analytical expression of the propagation field, as done in Ref. [33], the hard-edge aperture function $\Pi(x, y)$ is expanded as the sum of complex Gaussian functions with finite terms [33–35]:

$$\Pi(x, y) = \sum_{j=1}^{M} \sum_{l=1}^{M} B_j B_l \exp\left(-\frac{C_l x^2}{a^2} - \frac{C_j y^2}{b^2}\right), \tag{3}$$

where the complex constants B_j and C_l are the expansion and Gaussian coefficients, respectively, which can be obtained by optimization computation directly, while M is the number of complex Gaussian terms. Their values can be found in Table 1 of Ref. [33].

According to the vector angular spectrum representation of Maxwell's equations [20, 26–28], the diffracted plane wave propagating toward the half free space $z \ge 0$ is obtained from

$$\mathbf{E}(\mathbf{r}) = \int\int_{-\infty}^{\infty} \mathbf{A}(p, q) \exp(\mathrm{i}k\mathbf{s} \cdot \mathbf{r})\, \mathrm{d}p\, \mathrm{d}q. \tag{4}$$

Here $\mathbf{r} = x\mathbf{i} + y\mathbf{j} + z\mathbf{k}$ is the location vector, $\mathbf{s} = p\mathbf{i} + q\mathbf{j} + m\mathbf{k}$ and $m = \sqrt{1 - p^2 - q^2}$. And, the vector angular spectrum is represented as

$$\mathbf{A}(p, q) = A_x(p, q)\left(\mathbf{i} - \frac{p}{m}\mathbf{k}\right) + A_y(p, q)\left(\mathbf{j} - \frac{q}{m}\mathbf{k}\right), \tag{5}$$

while

$$\begin{pmatrix} A_x(p, q) \\ A_y(p, q \end{pmatrix} = \begin{pmatrix} \cos\alpha \\ \sin\alpha \end{pmatrix} A_0(p, q), \tag{6}$$

where

$$\begin{aligned} A_0(p, q) &= \frac{1}{\lambda^2} \int_{-\infty}^{\infty} \int_{-\infty}^{\infty} \exp\left(-\frac{x^2 + y^2}{w_0^2}\right) \Pi(x, y) \\ &\quad \times \exp\big[-\mathrm{i}k(px + qy)\big]\, \mathrm{d}x\, \mathrm{d}y \\ &= \frac{w_0^2}{4\pi} \sum_{l}^{M} \sum_{j}^{M} \frac{B_l B_j}{\sqrt{w_{la} w_{jb}}} \\ &\quad \times \exp\left[-\frac{k^2 w_0^2}{4}\left(\frac{p^2}{w_{la}} + \frac{q^2}{w_{jb}}\right)\right], \end{aligned} \tag{7}$$

with $w_{la} = 1 + C_l w_0^2/a^2$ and $w_{jb} = 1 + C_j w_0^2/b^2$.

The longitudinal component originates from the transversality condition of the optical field $\nabla \cdot \mathbf{E}(\mathbf{r}) = 0$, where the dot denotes the scalar product. According to the vectorial structure of the electromagnetic wave [20, 26–28], two unit vectors $\mathbf{e}_1$ and $\mathbf{e}_2$ can be defined in the frequency domain:

$$\begin{aligned} \mathbf{e}_1 &= \frac{q}{\sqrt{p^2 + q^2}}\mathbf{i} - \frac{p}{\sqrt{p^2 + q^2}}\mathbf{j}, \\ \mathbf{e}_2 &= \frac{pm}{\sqrt{p^2 + q^2}}\mathbf{i} + \frac{qm}{\sqrt{p^2 + q^2}}\mathbf{j} - \sqrt{p^2 + q^2}\mathbf{k}. \end{aligned} \tag{8}$$

In this system, the vector angular spectrum $\mathbf{A}(p, q)$ can be decomposed into two terms:

$$\mathbf{A}(p, q) = \big[\mathbf{A}(p, q) \cdot \mathbf{e}_1\big]\mathbf{e}_1 + \big[\mathbf{A}(p, q) \cdot \mathbf{e}_2\big]\mathbf{e}_2. \tag{9}$$

Based on the vectorial structure of a non-paraxial electromagnetic beam, the propagating electric field of non-paraxial vectorial beams can be written as a sum of two terms, that is,

$$\mathbf{E}(\mathbf{r}) = \mathbf{E}_{\mathrm{TE}}(\mathbf{r}) + \mathbf{E}_{\mathrm{TM}}(\mathbf{r}), \tag{10}$$

where

$$\begin{aligned} \mathbf{E}_X(\mathbf{r}) &= \int_{-\infty}^{\infty} \int_{-\infty}^{\infty} \mathbf{A}_X^E(p, q, m) \exp(\mathrm{i}k\mathbf{s} \cdot \mathbf{r})\, \mathrm{d}p\, \mathrm{d}q \\ &\quad \text{for } X = \mathrm{TE}, \mathrm{TM} \end{aligned} \tag{11}$$

and

$$\mathbf{A}_{\mathrm{TE}}^{E}(p,q,m) = (\mathbf{A}\cdot\mathbf{e}_1)\mathbf{e}_1 = \frac{(q\cos\alpha - p\sin\alpha)}{p^2+q^2}(q\mathbf{i}-p\mathbf{j})A_0(p,q), \tag{12}$$

$$\mathbf{A}_{\mathrm{TM}}^{E}(p,q,m) = (\mathbf{A}\cdot\mathbf{e}_2)\mathbf{e}_2 = \frac{(p\cos\alpha + q\sin\alpha)}{m(p^2+q^2)} \times \left[m(p\mathbf{i}+q\mathbf{j}) - (p^2+q^2)\mathbf{k}\right]A_0(p,q). \tag{13}$$

Similarly, the propagating magnetic field of vectorial beams can also be divided into the corresponding TE and TM terms:

$$\mathbf{H}(\mathbf{r}) = \mathbf{H}_{\mathrm{TE}}(\mathbf{r}) + \mathbf{H}_{\mathrm{TM}}(\mathbf{r}), \tag{14}$$

where

$$\mathbf{H}_X(\mathbf{r}) = \sqrt{\frac{\varepsilon}{\mu}}\int_{-\infty}^{\infty}\int_{-\infty}^{\infty}\mathbf{A}_X^H\exp(\mathrm{i}k\mathbf{s}\cdot\mathbf{r})\,\mathrm{d}p\,\mathrm{d}q \quad \text{for } X = \mathrm{TE},\mathrm{TM} \tag{15}$$

and

$$\mathbf{A}_{\mathrm{TE}}^{H}(p,q,\gamma) = (\mathbf{A}\cdot\mathbf{e}_1)\mathbf{e}_2 = \frac{(q\cos\alpha - p\sin\alpha)}{p^2+q^2} \times \left[\gamma(p\mathbf{i}+q\mathbf{j}) - (p^2+q^2)\mathbf{k}\right]A_0(p,q), \tag{16}$$

$$\mathbf{A}_{\mathrm{TM}}^{H}(p,q,\gamma) = (\mathbf{A}\cdot\mathbf{e}_2)\mathbf{e}_1 = \frac{(p\cos\alpha + q\sin\alpha)}{\gamma(p^2+q^2)} \times (q\mathbf{i}-p\mathbf{j})A_0(p,q). \tag{17}$$

As stated in (12) and (17), the TE or TM term represents that the longitudinal component of the electric field $\mathbf{E}_{\mathrm{TE}}(\mathbf{r})$ or the magnetic field $\mathbf{H}_{\mathrm{TM}}(\mathbf{r})$ is equal to zero, respectively.

It is well known that, provided that z is large enough, i.e. in the far-field regime, the evanescent plane waves completely disappear. Although in (11) and (15) the integrand functions have a sum form consisting of complex functions of finite terms, as pointed out in Ref. [30] in the far-field regime the condition $kr = k\sqrt{x^2+y^2+z^2} \to \infty$ is satisfied and the method of stationary phase is still applicable [15, 26]. Therefore, the analytical electromagnetic field of the TE and TM terms in the far-field regime can be expressed as

$$\mathbf{E}_X(\mathbf{r}) = -\frac{\mathrm{i}\lambda z}{r^2}\mathbf{A}_X^E\left(\frac{x}{r},\frac{y}{r},\frac{z}{r}\right)\exp(\mathrm{i}kr), \quad X = \mathrm{TE},\mathrm{TM} \tag{18}$$

$$\mathbf{H}_X(\mathbf{r}) = -\sqrt{\frac{\varepsilon}{\mu}}\frac{\mathrm{i}\lambda z}{r^2}\mathbf{A}_X^H\left(\frac{x}{r},\frac{y}{r},\frac{z}{r}\right)\exp(\mathrm{i}kr), \quad X = \mathrm{TE},\mathrm{TM}. \tag{19}$$

3 Energy flux densities in the far field

The energy flux densities at the $z =$ constant plane are given by the z component of their time-average Poynting vector. The energy flux densities at the far-field $z =$ constant plane turn out to be

$$\mathbf{S}_{\mathrm{TE}z} = \frac{1}{2}\langle\mathbf{E}_{\mathrm{TE}}^{*}\times\mathbf{H}_{\mathrm{TE}}\rangle_z = \frac{\lambda^2}{2}\sqrt{\frac{\varepsilon}{\mu}}\frac{z^3}{r^5}\left|A_0\left(\frac{x}{r},\frac{y}{r}\right)\right|^2\sin^2(\theta-\alpha), \tag{20}$$

$$\mathbf{S}_{\mathrm{TM}z} = \frac{1}{2}\langle\mathbf{E}_{\mathrm{TM}}^{*}\times\mathbf{H}_{\mathrm{TM}}\rangle_z = \frac{\lambda^2}{2}\sqrt{\frac{\varepsilon}{\mu}}\frac{z}{r^3}\left|A_0\left(\frac{x}{r},\frac{y}{r}\right)\right|^2\cos^2(\theta-\alpha), \tag{21}$$

where $\theta = \tan^{-1}(y/x)$, the angle brackets indicate a time average and the asterisk * denotes a complex conjugation.

At first, making use of (19) and (20), the numerical evaluations are done and it is found that, for a linearly polarized GB, when the aperture size is larger than the beam width, the far-field patterns of $S_{\mathrm{TE}z}$ and $S_{\mathrm{TM}z}$ are always two-lobe or eight-figure structures with the same size whose origins are always mutually orthogonal. The pattern of the total energy flux density $S_z = S_{\mathrm{TE}z} + S_{\mathrm{TM}z}$ is similar to the input GB spot. Besides, it is also true that the influence of a rectangular aperture with much larger size compared with the beam width on the vectorial structure of GBs is negligible, which will be put aside in the remaining part.

When the aperture size is smaller than the beam width, the long side of the larger patterns of $S_{\mathrm{TE}z}$ or $S_{\mathrm{TM}z}$ is always perpendicular to the long side of the rectangular aperture, while the pattern of S_z closes to an elliptical GB spot, which can be seen from Fig. 1. We can also see that the spot sizes associated with TE or TM terms sensitively depend on the aperture parameters a and b for a given beam width. For example, for a square aperture ($a = b$) the spot sizes of $S_{\mathrm{TE}z}$ and $S_{\mathrm{TM}z}$ seem alike except for their origins. However, the pattern of $S_{\mathrm{TM}z}$ becomes larger for $b > a$ but is smaller for $a > b$ compared with that of $S_{\mathrm{TE}z}$ when $\alpha = 0$.

Next, the energy flux density patterns in the far-field regime also rely on the polarized angle α. In fact, α also

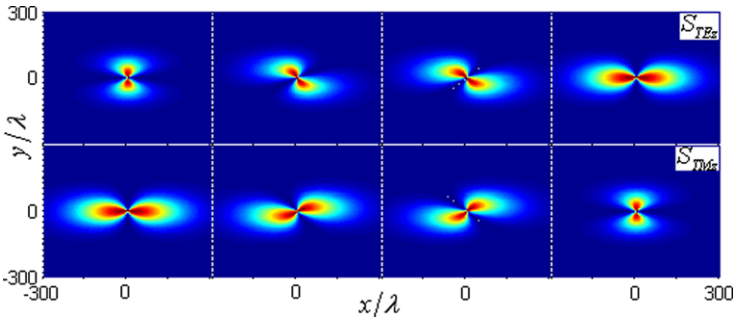

Fig. 2 Energy flux densities $S_{\mathrm{TE}z}$ (*upper row*) and $S_{\mathrm{TM}z}$ (*lower row*) of a GB at $z = 500\lambda$, $w_0 = 3\lambda$, $a = 2\lambda$, $b = 10\lambda$ and $\alpha = 0, \pi/6, \pi/4, \pi/2$ (from left to right), respectively

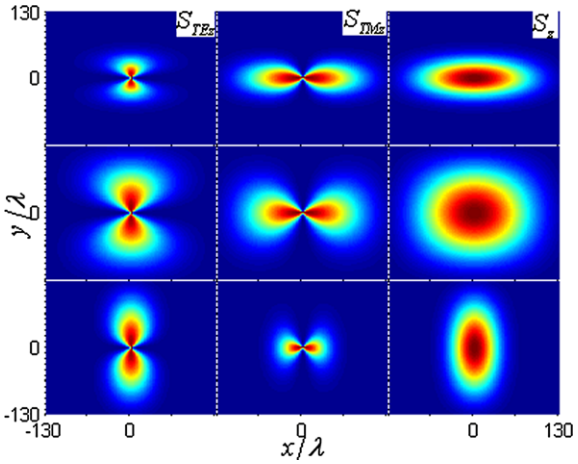

Fig. 1 Energy flux densities $S_{\mathrm{TE}z}$ (*left*), $S_{\mathrm{TM}z}$ (*middle*) and S_z (*right*) of vectorial GBs with $z = 3000\lambda$, $\alpha = 0$, $w_0 = 30\lambda$ and $(a, b)/w_0 = (\frac{1}{2}, 2), (\frac{1}{2}, \frac{1}{2}), (2, \frac{1}{2})$ (*from top to bottom*), respectively

represents the relative origin between the long side of the rectangular aperture and the polarization direction of the incident GB. $\alpha = 0$ or $\alpha = \pi/2$ respectively corresponds to these directions being mutually orthogonal or parallel. The far-field pattern of $S_{\mathrm{TM}z}$ is larger for $\alpha = 0$ and the spot of $S_{\mathrm{TE}z}$ becomes larger for $\alpha = \pi/2$, as well as the origin of the larger figure of eight and the long axis of the total energy flux spot being always perpendicular to the long side of the rectangular aperture. Moreover, for other polarization directions, the spots of $S_{\mathrm{TE}z}$ and $S_{\mathrm{TM}z}$ are twisted and the spot sizes change with α variation. Especially, when $\alpha = \pi/4$ the sizes of the twisted spots associated with TE and TM terms are alike for a linearly polarized GB diffracted by a rectangular aperture except for their origins, as shown in Fig. 2.

4 Energy fluxes in the far field

In order to accurately measure the energy fluxes associated with TE and TM terms, the quantities

$$P_X = \frac{\iint S_{Xz}\,\mathrm{d}x\,\mathrm{d}y}{\iint (S_{\mathrm{TE}z} + S_{\mathrm{TM}z})\,\mathrm{d}x\,\mathrm{d}y} \quad X = \mathrm{TE\ or\ TM} \tag{22}$$

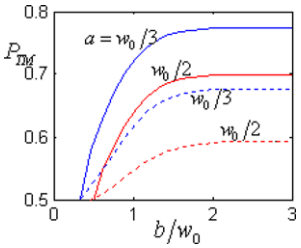

Fig. 3 Variations of P_{TM} with b for $\alpha = 0$, $z = 3000\lambda$. $w_0 = 30\lambda$ (*solid line*) and $w_0 = 10\lambda$ (*dashed line*)

are calculated, which represent the ratios of the energy fluxes related to TE or TM terms in the whole energy flux. The evaluations performed indicate that the energy fluxes associated with TE and TM terms rely on the rectangular aperture configuration and the angle α. Like a circular GB without an aperture, $P_{\mathrm{TE}} = P_{\mathrm{TM}} = 0.5$ always holds true for a square aperture ($a = b$), that is, the field components of TM and TE terms have the same share in the whole far field.

In this paper, only the variation of P_{TM} is studied in detail because $P_{\mathrm{TE}} = 1 - P_{\mathrm{TM}}$ can be similarly treated. The deviation of P_{TM} from 0.5 mainly depends on the aspect ratio b/a of the rectangular aperture and the angle α. For example, for $\alpha = 0$ and given a being the short side of the rectangular aperture, P_{TM} (> 0.5) increases with an increase of the long side b of the rectangular aperture when b is sufficiently small, as shown in Fig. 3. Roughly, after $b > 2w_0$ P_{TM} seems unchanged, which is reasonable because the contribution from the farther regime than $2w_0$ is negligible due to the distribution feature of GBs. However, the variation of P_{TM} just reverses when b is the short side of the rectangular aperture. In other words, in the far-field regime the TE component is dominant when the polarization direction and the long side of the rectangular aperture are parallel and the TM component becomes the leading one when they are mutually orthogonal. Figure 4 displays the dependence of P_{TM} on the polarization angle α and we can see that $P_{\mathrm{TE}} = P_{\mathrm{TM}} = 0.5$ always occurs when $\alpha = \pi/4$ or $3\pi/4$ even for a rectangular aperture, at which the corresponding density patterns shown in Fig. 2 seem alike, too.

Additionally, the parameters

$$C_Y^b = \iint S_Y^{b\geq a}\,\mathrm{d}x\,\mathrm{d}y \Big/ \iint S_Y^{a=b}\,\mathrm{d}x\,\mathrm{d}y$$
$$(Y = \mathrm{TE}\ z,\ \mathrm{TM}z\ \mathrm{and}\ z) \tag{23}$$

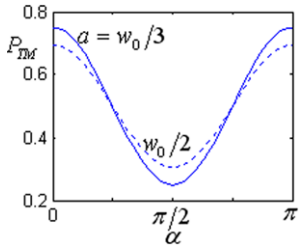

Fig. 4 Variations of P_{TM} with the polarization angle α for $b/a = 4$, $z = 3000\lambda$, $w_0 = 30\lambda$

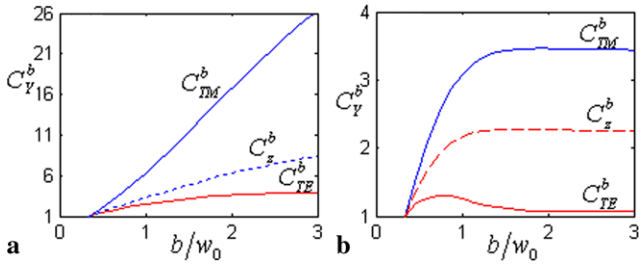

Fig. 5 Relations of C_Y^b with b for $z = 3000\lambda$, $a = w_0/3$, $\alpha = 0$. (**a**) $w_0 = 6\lambda$ and (**b**) $w_0 = 30\lambda$

are also calculated in order to determine the far-field energy flux difference between a rectangular aperture ($b \geq a$) and a square aperture ($a = b$) with the same incident field amplitude. Figure 5 shows the calculation results. From this figure and in combination with the energy flux distributions plotted in Figs. 1 and 2, it can be seen that the larger energy fluxes associated with S_z and S_{TM} and smaller spots can be achieved for a rectangular aperture with a larger b. The energy flux increase is rational because the light energy rises with an increase of the aperture area compared with a square aperture for small b. Therefore, by making use of the rectangular aperture diffraction of GBs, it is possible to obtain an isolated TE or TM field with a smaller spot and a larger energy flux so as to further enhance the density of optical storage.

Finally, the fact that the spot sizes of the energy flux densities or the energy fluxes of TE and TM terms depend on the aperture configuration may be applied to implement information encoding and transmission in free space. The same or different spot sizes or energy fluxes of TE and TM components may be designated as a bit '1' or '0', respectively (the notation S and D is used to indicate the same and different sizes or energy fluxes in the row under the data row in Fig. 6). Thus, by properly adjusting the aperture shape, whether the spot sizes or the energy fluxes are the same or not can be controlled accordingly, as indicated in the bottom row of Fig. 6. Actually, this method is direct and easier to implement, and no incident light source's properties need to be modulated to control the energy flux density spot sizes or the energy fluxes, which is very similar to that advanced in Ref. [36]. We consider that the spot sizes or the energy fluxes are more suitable to be determined because they are

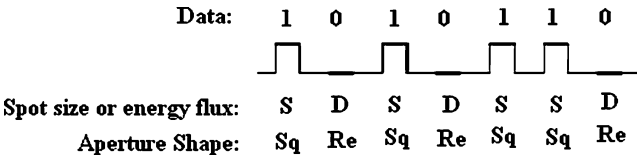

Fig. 6 Illustration for the data encoding and information transmission by controlling the aperture shape. Comparison of the energy flux density spot sizes or the energy fluxes of the TE and TM terms; the same size or energy flux (*S*) is associated with a bit of information such as '*1*' and the different size or energy flux (*D*) is associated with a bit '*0*', where '*Sq*' or '*Re*' respectively represents a square or a rectangular aperture

easy to be measured with a spot meter or an optical power meter, as in some experiments.

5 Conclusions

With the help of the angular spectrum representation and the Gaussian function expansions of the hard-edge aperture function, the vectorial structure of a GB diffracted by a rectangular aperture is analyzed in detail. Based on the numerical calculations it is found that, like the beam propagation without an aperture, the TM and TE component fields are not affected when the aperture size is larger than the beam width and share the same component in the whole far field. They also hold equal shares when the aperture is a square one with arbitrary α or a rectangular one with polarization angle $\alpha = \pi/4$ and $3\pi/4$ even when the aperture size is smaller than the beam width. Compared with the TE field, the TM field is a major component when the polarization direction and the long side of the rectangular aperture are mutually orthogonal but reverses when they are parallel. Because the far-field patterns bear information concerning the rectangular aperture configuration and polarization direction of an incident GB, smaller spots and larger energy fluxes can be achieved with a rectangular aperture in comparison with a square aperture; therefore, the discussion is helpful to understand the theoretical aspects of apertured GBs. Other potential applications of the TE and TM terms deserve further investigation besides the fact that an isolated TE or TM term may be re-focused to improve the density of optical storage. For example, a scheme is proposed to implement information encoding and transmission in free space.

References

1. A.E. Siegman, *Lasers* (University Science Books, Mill Valley, 1986)
2. K. Tanaka, K. Yoshida, M. Taguchi, Appl. Opt. **27**, 1310 (1988)
3. G.P. Zhao, X.L. Ji, B.D. Lu, Optik **114**, 241 (2003)
4. B.D. Lu, B. Zhang, J. Mod. Opt. **40**, 1731 (1993)
5. B.D. Lu, S.R. Luo, B. Zhang, Opt. Commun. **164**, 1 (1999)

6. D. Ding, X. Liu, J. Opt. Soc. Am. A **16**, 1286 (1999)
7. B.D. Lu, S.R. Luo, J. Mod. Opt. **48**, 2169 (2001)
8. Z.R. Mei, J.G. Gu, Appl. Phys. B, Lasers Opt. **99**, 571 (2010)
9. K. Duan, B.B. Lu, Opt. Express **11**, 1474 (2003)
10. Y.J. Zhang, Opt. Commun. **248**, 317 (2005)
11. M. Lax, W.H. Louisell, W.B. McKnight, Phys. Rev. A **11**, 1365 (1975)
12. L.W. Davis, Phys. Rev. A **19**, 1177 (1979)
13. S.R. Seshadri, J. Opt. Soc. Am. A **15**, 2712 (1998)
14. A. Wunsche, J. Opt. Soc. Am. A **9**, 765 (1992)
15. W.H. Carter, J. Opt. Soc. Am. A **62**, 1195 (1972)
16. S.R.S. Seshadri, Opt. Lett. **28**, 595 (2003)
17. B. Lu, K. Duan, Opt. Lett. **28**, 2440 (2004)
18. C.W. Zheng, Y.J. Zhang, L. Wang, Opt. Laser Technol. **39**, 598 (2007)
19. A. Doicu, T. Wriedt, Opt. Commun. **136**, 114 (1997)
20. R.M. Herrero, P.M. Mejıas, S. Bosch, A. Carnicer, J. Opt. Soc. Am. A **18**, 1678 (2001)
21. A.S. Marathay, J.F. McCalmont, J. Opt. Soc. Am. A **18**, 2585 (2001)
22. C.G. Chen, P.T. Konkola, J. Ferrera, R.K. Heilmann, M.L. Schattenburg, J. Opt. Soc. Am. A **19**, 404 (2002)
23. H.M. Guo, J.B. Chen, S.L. Zhuang, Opt. Express **14**, 2095 (2006)
24. R.M. Herrero, P.M. Mejıas, Opt. Express **16**, 9021 (2008)
25. R.M. Herrero, P.M. Mejıas, S. Bosch, Opt. Commun. **281**, 265 (2008)
26. G.H. Wu, Q.H. Lou, J. Zhou, Opt. Express **16**, 6417 (2008)
27. D.M. Deng, Q. Guo, Opt. Lett. **32**, 2711 (2007)
28. G.Q. Zhou, Opt. Lett. **31**, 2616 (2006)
29. G.Q. Zhou, Y.Z. Ni, Z.W. Zhang, Opt. Commun. **272**, 32 (2007)
30. H.Q. Tang, X.G. Li, G.Q. Zhou, K.C. Zhu, Opt. Commun. **282**, 478 (2009)
31. G.Q. Zhou, X.X. Chu, J. Zheng, Opt. Commun. **281**, 1929 (2008)
32. P.S. Liu, B.D. Lu, Opt. Laser Technol. **39**, 741 (2007)
33. J.J. Wen, M.A. Breazeale, J. Acoust. Soc. Am. **83**, 1752 (1988)
34. Y. Cai, L. Hu, Opt. Lett. **31**, 685 (2006)
35. F. Wang, Y. Cai, Q. Lin, J. Opt. Soc. Am. A **25**, 2001 (2008)
36. P. Han, J. Opt. Soc. Am. A **26**, 473 (2009)